Spatially Similar Surface Energy Flux Perturbations due to Greenhouse Gases and Aerosols

Geeta G. Persad*[1], Yi Ming[2], and V. Ramaswamy[2]

* Corresponding Author: G.G. Persad, Program in Atmospheric and Oceanic Sciences, Princeton University, 201 Forrestal Road, Princeton, NJ 08540, USA. (gpersad@princeton.edu)
[1] Program in Atmospheric and Oceanic Sciences, Princeton University, Princeton, NJ, USA.
[2] NOAA Geophysical Fluid Dynamics Laboratory, Princeton, NJ, USA.

Recent studies suggest that, despite distinct geographic distributions of top-of-the-atmosphere radiative forcing, anthropogenic greenhouse gases and aerosols give rise to similar patterns of climate response (though of opposite sign) in fully atmosphere-and-ocean coupled general circulation model simulations. The surface energy flux perturbation, a crucial pathway by which atmospheric forcing is communicated to the ocean, may be a vital link in explaining the spatial similarities in the full atmosphere-and-ocean responses to disparate forcings. We here analyze the fast, atmosphere-only change in surface energy flux caused by present-day greenhouse gases versus aerosols to elucidate its role in shaping the subsequent slow, coupled response. We find that, although the two forcings are largely uncorrelated under clear-sky conditions at the top-of-the-atmosphere, their surface energy flux perturbation patterns are significantly anti-correlated. Our analysis highlights the common modes of atmospheric circulation and surface energy adjustment that are triggered by both greenhouse gas and aerosol forcings. These produce antisymmetric (i.e. symmetric, but of opposite sign) spatial patterns of surface sensible and latent heat flux variations in response to the two forcers, particularly over the winter-hemisphere oceans. Our results suggest that atmosphere-only processes are capable of achieving substantial homogenization within a given hemisphere in the climate response to disparate forcers on fast timescales, with implications for detection and attribution and for the understanding and prediction of the regional climate impacts of anthropogenic greenhouse gases and aerosols.

Although it has been demonstrated that the fully coupled response to greenhouse gases (GHGs) and aerosols have significant, though not complete, spatial pattern similarity, the mechanisms for pattern formation remain poorly characterized [e.g. Levy et al., 2008; Levy et

al., 2013; Xie et al., 2013]. Xie et al. [2013] suggest that the spatial similarities in the fully coupled response to GHGs and aerosols, analyzed in a subset of the Coupled Model Intercomparison Project Phase 5 (CMIP5) models, are strongly mediated by common patterns of ocean-atmosphere feedbacks that can be separated conceptually into a fast, atmosphere-only component and a slower, ocean-atmosphere coupled component. The degree of spatial similarity in the climate response to GHGs versus aerosols has significant implications for questions in the detection and attribution of anthropogenic climate change [Bindoff et al., 2013 and references therein] and for our understanding of the transient climate response to heterogeneous versus homogeneous forcers [e.g. Shindell, 2014]. It is thus vital to characterize the fast and slow mechanisms via which the spatial patterns of response are produced.

We here probe the fast, atmosphere-only component of the formation of the spatial patterns of response to present-day GHGs and aerosols in an atmospheric general circulation model—a crucial intermediate step toward understanding the fully coupled response. We find that the top-of-the-atmosphere (TOA), all-sky, effective radiative forcings (ERFs) [Myhre et al., 2013] of GHGs and aerosols are only weakly anti-correlated (R=-0.42) in our simulations, comparable to values found in other studies [e.g. Xie et al., 2014]. ERF is calculated as the difference in TOA radiative flux between simulations with and without the forcing agent after the atmospheric and land temperatures have been allowed to re-equilibrate. Aerosols' TOA ERF pattern (Fig. 1b), due to aerosols' short atmospheric lifetime, is dependent on regional factors like surface albedo and the location of emissions, and is concentrated in the Northern Hemisphere. GHGs' TOA ERF pattern, meanwhile, is by-and-large hemispherically symmetric and uniformly distributed (Fig. 1a).

The clear-sky TOA ERF of GHGs and aerosols is essentially uncorrelated (R_{clr} = -0.09), suggesting that the all-sky TOA ERF correlation is strongly influenced by clouds through the so-called "cloud masking" effect [e.g. Soden et al., 2004]. Furthermore, the all-sky TOA ERF includes the radiative effects of rapid cloud adjustments [Myhre et al., 2013]. The spatial anti-correlation of the change in low cloud cover between the two runs (R = -0.52) is comparable to that for the all-sky TOA ERF, indicating that the latter can also be explained partially by antisymmetric (i.e. symmetric, but of opposite sign) cloud changes in response to the two forcers.

The spatial differences between the TOA ERF due to GHGs and that due to aerosols, however, are not maintained in the surface energy flux perturbation to each. The pattern of surface energy flux perturbation (ΔS, defined as the change in total surface energy flux, composed of radiative shortwave and longwave, latent, and sensible energy) in response to the two forcers is more strongly anti-correlated (R=-0.57) than the clear-sky TOA ERF (R=-0.09), indicating a process of homogenization between the TOA perturbation and the surface perturbation. Because the surface energy balance over land rapidly re-equilibrates due to the low effective heat capacity of the land surface, ΔS is near zero for all land surfaces by necessity. Thus, the anti-correlation of ΔS manifests almost entirely over the ocean. The oceanic surface energy balance is not constrained to re-equilibrate on atmosphere-only timescales, and as such will primarily reflect the atmospheric conditions setting surface fluxes.

ΔS can be construed as an intermediary between the TOA atmospheric perturbation of a forcing agent and the ocean response thereto, and is thus a telling manifestation of the fast, atmosphere-only pathway for fully atmosphere-and-ocean coupled response pattern formation. The annual-mean, global-mean ΔS correlation between GHGs and aerosols emerges most strongly in the surface latent and sensible heat flux components of the surface energy balance

74 (Table 1). In contrast, the surface radiative (shortwave and longwave) flux change is little
75 correlated (R=-0.26), indicating that neither climatological cloud masking nor cloud change is
76 responsible for the spatial similarities in ΔS. The strongest anti-correlation occurs largely over
77 the winter-hemisphere extratropical oceans, as indicated by the seasonal and latitudinal
78 decomposition of ΔS (Table 1), and is driven by antisymmetric wave-like patterns in the surface
79 latent and sensible heat flux change in response to each forcer (Fig. 1c,d).
80 The common pattern of surface heat flux change in response to each forcer is a
81 manifestation of a wave perturbation to the atmospheric circulation that is produced by both
82 GHGs and aerosols. Over the extratropical oceans, a barotropic stationary Rossby wave
83 perturbation to the atmospheric flow, consistent with the wave pattern in surface heat fluxes, is
84 evident in alternating positive and negative anomalies collocated in sea level pressure (SLP) and
85 in geopotential height at the 500-hpa pressure level (Z_{500}) for both forcers (Fig. 2a,b). The
86 annual-mean patterns of SLP and Z_{500} perturbations due to GHGs and aerosols are correlated at
87 R=-0.53 and R=-0.49, respectively. Surface winds and temperature and specific humidity
88 gradients between the surface and air, the primary controllers of surface heat fluxes, also exhibit
89 qualitative wave patterns in the extratropics (not shown)—a consequence of the changes in
90 extratropical atmospheric flow demonstrated in the SLP and Z_{500} anomalies.
91 Rossby wave perturbations to the extratropical atmospheric flow can occur via wave
92 sources located either in the extratropics or in the tropics. Wave excitation within the extratropics
93 can result from changes in extratropical land-sea thermal and diabatic heating contrast caused by
94 land surface temperature adjustments to forcing under the constraint of fixed sea surface
95 temperatures [Held et al., 2002; Ming et al., 2011]. Excitation of extratropical waves from within
96 the tropics, meanwhile, can occur due to changes in tropical deep convection and precipitation

97 (and thus atmospheric latent heating), the signal from which then propagates into the extratropics
98 [Sardeshmukh and Hoskins, 1987; Held and Soden, 2006; Vecchi and Soden, 2007; Ming and
99 Ramaswamy, 2011].

100 Greenhouse gases and aerosols trigger these wave sources antisymmetrically. In the
101 extratropics, the location of the landmasses serves as a potent fixed wave source in the presence
102 of both forcers. The wintertime land-sea contrast ($T_{L/S}$, quantified as the climatologically
103 negative wintertime hemispheric-mean difference between land and ocean surface temperatures)
104 increases in the presence of aerosols ($\Delta T_{L/S}$ = -0.15 K for the Northern Hemisphere, -0.006 K for
105 the Southern Hemisphere) and decreases in the presence of GHGs ($\Delta T_{L/S}$ = 0.31 K for the
106 Northern Hemisphere, 0.037 for the Southern Hemisphere). This perturbation to the
107 climatological land-sea contrast constitutes a diabatic heating anomaly that acts as an
108 extratropical source of Rossby waves [e.g. Held et al., 2002]. The surface temperature response
109 to GHGs and aerosols (Fig. 2c,d) is constrained to land in these prescribed sea surface
110 temperature (SST) runs. However, the land surface temperature response to the two forcers is
111 highly anti-correlated (R = -0.71), likely constrained by local surface energy availability
112 [Andrews et al., 2009] and regional sensitivities and feedbacks that are largely forcing
113 independent [Armour et al., 2013].

114 In the tropics, changes in deep tropical (20°S-20°N) precipitation due to GHGs and
115 aerosols can also act as a source for extratropical Rossby waves. The fact that the simulated
116 precipitation changes are indeed antisymmetric (R=-0.53) (Fig. 2e,f) may contribute to the
117 similar extratropical wave patterns. Interestingly, it is not straightforward why the two forcers
118 would give rise to antisymmetric precipitation changes. In fact, a thermodynamic scaling
119 argument suggests the opposite: under fixed-SST conditions, both GHGs and aerosols increase

tropospheric absorption of radiative energy, via increased absorption of longwave radiation in the case of GHGs and of shortwave radiation in the case of aerosols, and thus have suppressing effects on tropical mean precipitation [e.g. Roeckner et al., 1999; Allen and Ingram, 2002; Held and Soden, 2006; Ming et al., 2010]. Indeed, in our simulations, both forcers decrease tropical mean precipitation (by -0.89% for present-day GHGs and -1.2% for present-day aerosols). In our view, the antisymmetric spatial pattern of these precipitation reductions is driven mainly by the opposite land-sea surface temperature contrast patterns (Fig. 2c,d) and monsoonal circulation changes, which are dynamical in nature.

Our analysis of the mechanisms of surface pattern correlation demonstrates that the atmospheric circulation is an efficient homogenizer of heterogeneous forcings, even under fixed-SST conditions. Indeed, a simple energy balance analysis allows us to argue this based on energetic constraints alone. Because land surface and atmospheric energy perturbations rapidly equilibrate to zero, the total ocean surface energy perturbation ($\Delta R^{O}_{surf} + \Delta H^{O}_{surf}$, with ΔR and ΔH denoting the radiative and heat components, respectively) must equal the TOA ERF over oceans (ERF^{O}) plus that over land (ERF^{L}) in the global mean: $\Delta R^{O}_{surf} + \Delta H^{O}_{surf} = ERF^{O} + ERF^{L}$. Vertical radiative energy conservation dictates that the TOA ERF must equal the sum of the surface radiative perturbation (ΔR_{surf}) and any atmospheric absorption change ($ERF = \Delta R_{surf} + \Delta AA$). Thus, the surface heat flux perturbation over ocean will be equal to the total atmospheric absorption change over land and ocean plus the land surface radiative perturbation ($\Delta H^{O}_{surf} = \Delta AA^{O+L} + \Delta R^{L}_{surf}$), a balance that is evident in our simulations (Table 2). This coupling between the atmospheric and surface energetics over the land and the ocean dictates that most of the spatial heterogeneity in TOA forcing cannot be maintained and must be rapidly transformed (from radiation to heat) and redistributed (from the land surface and atmosphere to the ocean

surface) by the atmospheric circulation. This circulation adjustment process is fundamentally responsible for the similar ocean heat flux perturbation patterns between GHGs and aerosols.

Notably, the fast homogenization described in this work operates primarily within a single hemisphere. The ratio of Northern Hemisphere to Southern Hemisphere TOA ERF does not differ significantly from that of the surface energy perturbation (1.1 and 1.1, respectively, for GHGs and 2.8 and 3.0, respectively, for aerosols). Under fixed-SST conditions, the Hadley circulation, the main mode of atmospheric cross-equatorial transport, cannot readily respond to perturbations [e.g. Hill et al., 2014], constraining homogenization to within a given hemisphere.

The degree of similarity in the spatial pattern of the climate response to GHGs and aerosols has many implications for understanding and predicting the relative climate impacts of these forcers. Detection and attribution studies rely on spatial pattern as one component of the "fingerprint" of a given forcer, and similarity therein can result in a degradation of the ability to distinguish the signal from GHGs versus aerosols in climate phenomena [Bindoff et al., 2013 and references therein]. Further, our understanding of the regional distribution of present and future climate change relies on constraining the spatial structure of the response to heterogeneous forcers like aerosols versus homogeneous forcers like greenhouse gases [e.g. Shindell et al., 2010; Shindell and Faluvegi, 2009].

Our work reveals that, even on the short timescales captured in fixed-SST simulations, GHGs and aerosols can be expected to produce strongly correlated spatial patterns of change across a range of variables. This is enforced by the symmetric perturbation to the extratropical circulation provided by land-sea contrast, the spatial structure of which is fixed by the location of the landmasses and, thus, relatively insensitive to the structure of the initial forcing. Analysis of the spatial correlation of atmosphere-only change in response to greenhouse gases and aerosols

in a range of models will be crucial to improved understanding of this phenomenon. We have here presented a picture of the atmosphere-only dynamical and thermodynamical mechanisms that drive these similarities in our model, providing a bridge to understanding the fully atmosphere-and-ocean coupled spatial patterns described by Xie et al. [2013] and others, and encourage continued analysis of this phenomenon in additional climate models.

Methods

Atmospheric General Circulation Model Simulations. All simulations in this study are conducted with a modified version of the Geophysical Fluid Dynamics Laboratory's AM2.1 Atmospheric General Circulation Model, which prescribes aerosol concentrations and has a prognostic treatment of aerosol indirect effects on liquid clouds [Ming and Ramaswamy, 2009]. We analyze the time-averaged values from a set of three simulations run for 7 years with sea surface temperatures fixed to a repeating climatological annual cycle and different configurations of atmospheric constituents: an all forcing run with all natural and anthropogenic levels varying according to their historical values from 1983-1989 (ALL_F); a run with anthropogenic aerosol concentrations set to 1860 values and all other forcers varying according to their historical values from 1983-1989 (1860_AERO); and a pre-industrial run with all forcers set to 1860 values (PI). Aerosol effects were derived from the ALL_F run minus the 1860_AERO run, and GHG effects were derived from the 1860_AERO run minus the PI run. Results were evaluated for robustness by conducting preliminary analysis on the first 3 and last 3 years of the model simulations separately. The signal is highly consistent between the two 3-year periods in the annual-mean and JJA, but there is greater variability in the DJF midlatitude signal (Supp. Table 1), as expected from the noisy nature of the Northern Hemisphere wintertime weather [e.g. Hurrell and

189 Deser, 2014]. Only features consistent between these two, effectively independent, samples are
190 considered in this analysis.

191 **Correlation Coefficients.** Pearson correlation coefficients are calculated via linear regression
192 with area-weighting. Scatterplots of all data were analyzed to ensure insensitivity to outliers and
193 qualitative linearity of relationships. All correlation values given are significant at the 95% level.

194 **Acknowledgements.** G. G. Persad is partially funded by National Science Foundation Graduate
195 Research Fellowship DGE -1148900.

196 **Author Contributions**

197 Y. M. and G. G. P. conceived the idea for this study, and Y. M. carried out the model
198 simulations. G. G. P. conducted the analysis and wrote the text, with comments and input from
199 Y. M. and V. R.

200

201 **References**

202 Andrews, Timothy, Piers M. Forster, & Jonathan M. Gregory. A Surface Energy Perspective on Climate Change.
203 *Journal of Climate* **22**, 2557–70 (2009).
204 Armour, Kyle C., Cecilia M. Bitz, & Gerard H. Roe. Time-Varying Climate Sensitivity from Regional Feedbacks.
205 *Journal of Climate* **26**, 4518–34 (2012).
206 Bindoff, N.L. *et al*. in *Climate Change 2013: The Physical Science Basis. Contribution of Working Group I to the*
207 *Fifth Assessment Report of the Intergovernmental Panel on Climate Change* (eds. Stocker, T.F. *et al*.)
208 (Cambridge University Press, 2013).
209 Geisler, John E., Maurice L. Blackmon, Gary T. Bates, and S. Muñoz. "Sensitivity of January Climate Response to
210 the Magnitude and Position of Equatorial Pacific Sea Surface Temperature Anomalies." *Journal of the*
211 *Atmospheric Sciences* 42, no. 10 (May 1, 1985): 1037–49. doi:10.1175/1520-
212 0469(1985)042<1037:SOJCRT>2.0.CO;2.
213 Held, I. M., & B. J. Soden. Robust Responses of the Hydrological Cycle to Global Warming. *Journal of Climate* **19**,
214 5686–99 (2006).
215 Held, Isaac M., Mingfang Ting, & Hailan Wang. Northern Winter Stationary Waves: Theory and Modeling. *Journal*
216 *of Climate* **15**, 2125-44 (2002).
217 Hill, Spencer A., Yi Ming, & Isaac M. Held. Mechanisms of Forced Tropical Meridional Energy Flux Change.
218 *Journal of Climate* (Early Online Release) (2014).
219 Hurrell, J. W. and C. Deser. Northern hemisphere climate variability during winter: Looking back on the work of
220 Felix Exner. *Meteorol. Z.*, in press (2014).
221 Levy, Hiram, M. Daniel Schwarzkopf, Larry Horowitz, V. Ramaswamy, & K. L. Findell. Strong Sensitivity of Late
222 21st Century Climate to Projected Changes in Short-Lived Air Pollutants. *Journal of Geophysical Research*
223 **113**, D06102 (2008).
224 Levy, Hiram, Larry W. Horowitz, M. Daniel Schwarzkopf, Yi Ming, Jean-Christophe Golaz, Vaishali Naik, & V.
225 Ramaswamy. The Roles of Aerosol Direct and Indirect Effects in Past and Future Climate Change. *Journal of*
226 *Geophysical Research: Atmospheres* **118**, 4521–32 (2013).

Ming, Yi, & V. Ramaswamy. Nonlinear Climate and Hydrological Responses to Aerosol Effects. *Journal of Climate* **22**, 1329–39 (2009).
———A Model Investigation of Aerosol-Induced Changes in Tropical Circulation. *Journal of Climate* **24**, 5125–33 (2011).
———Nonlocal Component of Radiative Flux Perturbation. *Geophysical Research Letters* **39**, L22706 (2012).
Ming, Y., V. Ramaswamy, & Gang Chen. A Model Investigation of Aerosol-Induced Changes in Boreal Winter Extratropical Circulation. *Journal of Climate* **24**, 6077–91 (2009).
Myhre, G. *et al*. in *Climate Change 2013: The Physical Science Basis. Contribution of Working Group I to the Fifth Assessment Report of the Intergovernmental Panel on Climate Change* (eds. Stocker, T.F. *et al*.) (Cambridge University Press, 2013).
Roeckner, E., L. Bengtsson, J. Feichter, J. Lelieveld, & H. Rodhe. Transient climate change simulations with a coupled atmosphere–ocean GCM including the tropospheric sulfur cycle, *J. Clim*., **12**, 3004–3032 (1999).
Sardeshmukh, Prashant, and Brian Hoskins. "The Generation of Global Rotational Flow by Steady Ideadlize Tropical Divergence." *Journal of Atmospheric Sciences* 45, no. 7 (October 29, 1987): 1228–51.
Shindell, Drew T. Inhomogeneous Forcing and Transient Climate Sensitivity. *Nature Climate Change* **4**, 274-277 (2014).
Shindell, Drew, Michael Schulz, Yi Ming, Toshihiko Takemura, Greg Faluvegi, and V. Ramaswamy. "Spatial Scales of Climate Response to Inhomogeneous Radiative Forcing." *Journal of Geophysical Research: Atmospheres* 115, no. D19 (2010): 110-120. doi:10.1029/2010JD014108.
Shindell, Drew, and Greg Faluvegi. "Climate Response to Regional Radiative Forcing during the Twentieth Century." *Nature Geoscience* 2, no. 4 (April 2009): 294–300. doi:10.1038/ngeo473.
Simmons, A. J., J. M. Wallace, and G. W. Branstator. "Barotropic Wave Propagation and Instability, and Atmospheric Teleconnection Patterns." *Journal of the Atmospheric Sciences* 40, no. 6 (June 1, 1983): 1363–92. doi:10.1175/1520-0469(1983)040<1363:BWPAIA>2.0.CO;2.
Soden, B. J., Broccoli, A. J., & Hemler, R. S. On the use of cloud forcing to estimate cloud feedback. *J. Clim.* **17**, 3661-3665 (2004).
Vecchi, Gabriel A., & Brian J. Soden. Global Warming and the Weakening of the Tropical Circulation."*J. Clim*. **20**, 4316–40 (2007).
Xie, Shang-Ping, Bo Lu, & Baoqiang Xiang. Similar Spatial Patterns of Climate Responses to Aerosol and Greenhouse Gas Changes. *Nature Geoscience* **6**, 828–32 (2013).

	Annual Mean	JJA	DJF
TOA Effective Radiative Forcing	-0.42	-0.34	-0.57
Clear-sky TOA ERF	-0.09	-0.08	-0.53
Tropics (20S-20N)	-0.32	-0.45	-0.53
Surface Flux Perturbation	-0.57	-0.55	-0.62
Tropics (20S-20N)	-0.55	-0.57	-0.60
NH Extratropics (20N-90N)	-0.67	-0.22	-0.64
SH Extratropics (20S-90S)	-0.45	-0.70	-0.61
Surface Radiative (SW+LW) Flux	-0.26	-0.22	-0.48
Surface Sensible Heat Flux	-0.58	-0.57	-0.61
Surface Latent Heat Flux	-0.45	-0.52	-0.58

Table 1| Spatial correlations of TOA Effective Radiative Forcing and Surface Flux Perturbations due to greenhouse gases versus aerosols.

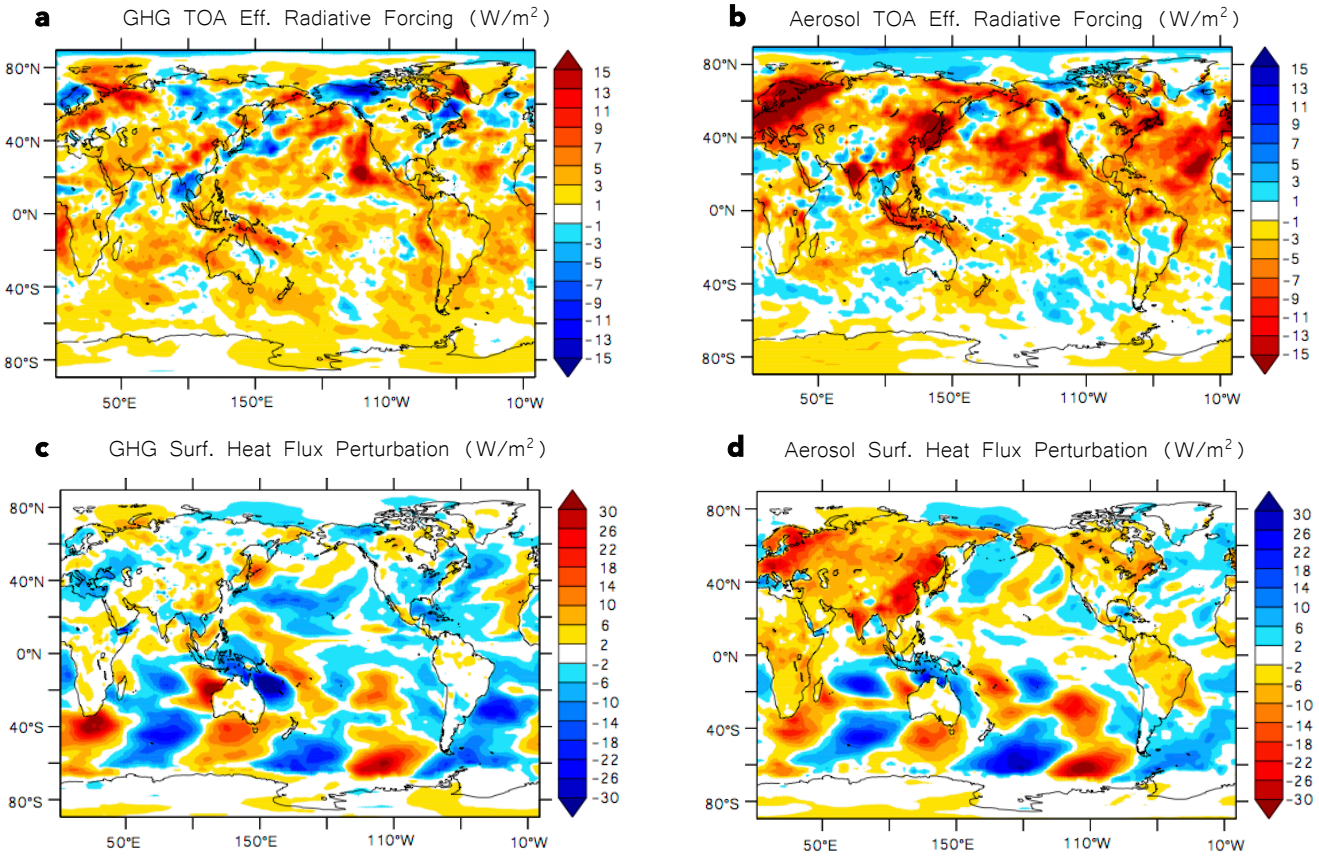

Figure 1| Spatial Similarities in TOA and Surface Forcing. a, b, JJA-mean TOA Effective Radiative Forcing due to **(a)** GHGs and **(b)** aerosols. **c,d,** JJA-mean surface heat flux perturbation due to **(c)** GHGs and **(d)** aerosols. (See supplementary material for DJF-mean values)

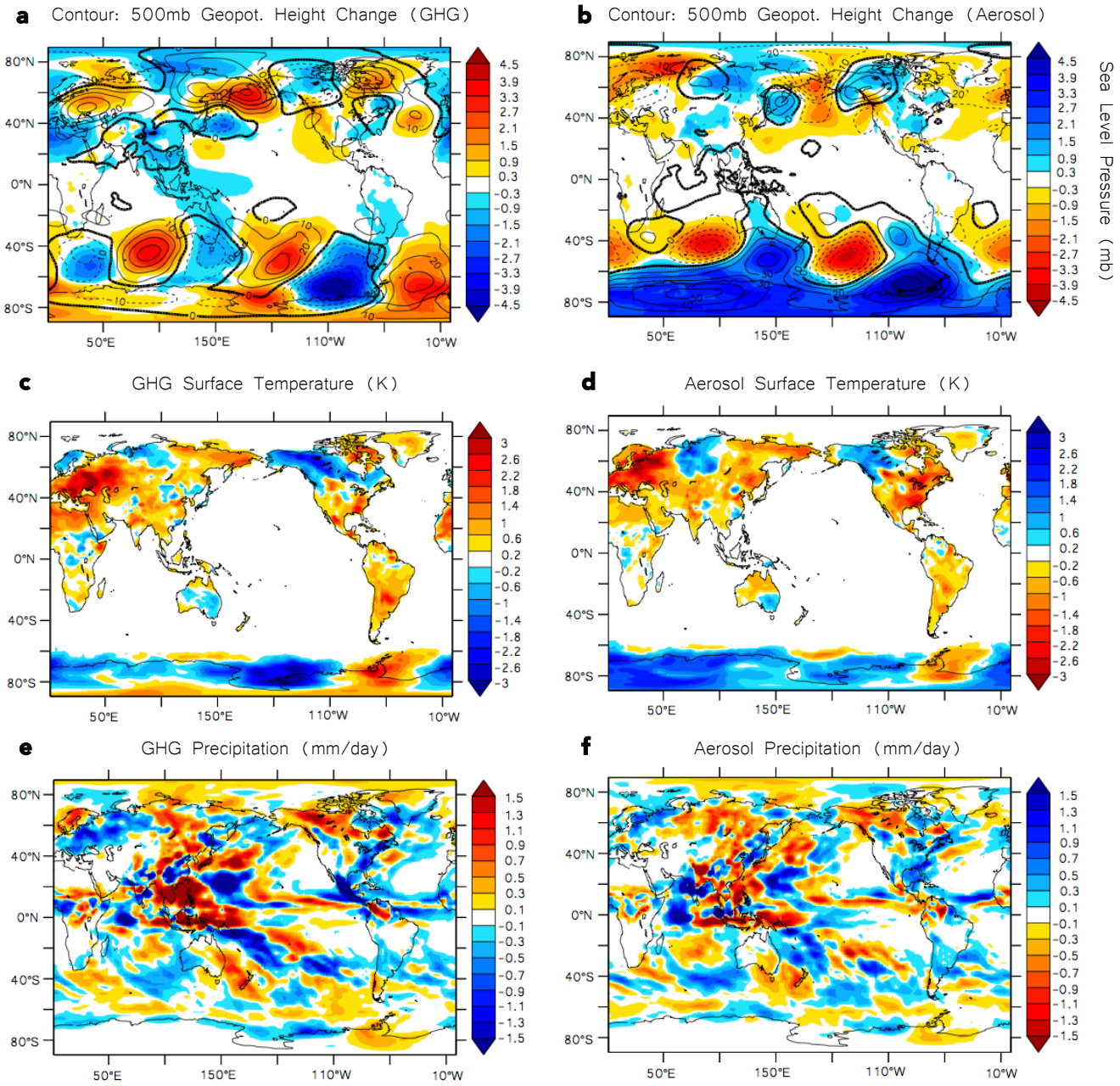

Figure 2| Spatially similar circulation changes. a-f, JJA-mean perturbations due to **(a, c, e)** GHGs and **(b, d, f)** aerosols in **(a, b)** 500mb geopotential height (contour interval, 5 m) and sea level pressure, **(c, d)** surface temperature and **(e, f)** precipitation.

Perturbation	Greenhouse Gas	Aerosol
Ocean surf. heat flux (ΔH^{O}_{surf})	0.58 (1.2)	0.22 (0.44)
Global atmos. abs. (ΔAA^{O+L})	0.53 (1.0)	0.86 (1.7)
Land surf. radiative flux (ΔR^{L}_{surf})	0.083 (0.16)	-0.68 (-1.3)
Ocean surf. radiative flux (ΔR^{O}_{surf})	0.45 (0.89)	-1.3 (-2.5)

Table 2| Annual-mean perturbations to energy balance terms due to present-day GHGs and aerosols in 10^{15} Watts (globally averaged in W/m^2).[1]

[1]Heat flux terms are positive upward, radiative flux terms are positive downward, atmospheric absorption terms are positive into the atmospheric column.

Supplement to Spatially Similar Surface Energy Flux Perturbations due to Greenhouse Gases and Aerosols

Geeta G. Persad, Yi Ming, and V. Ramaswamy

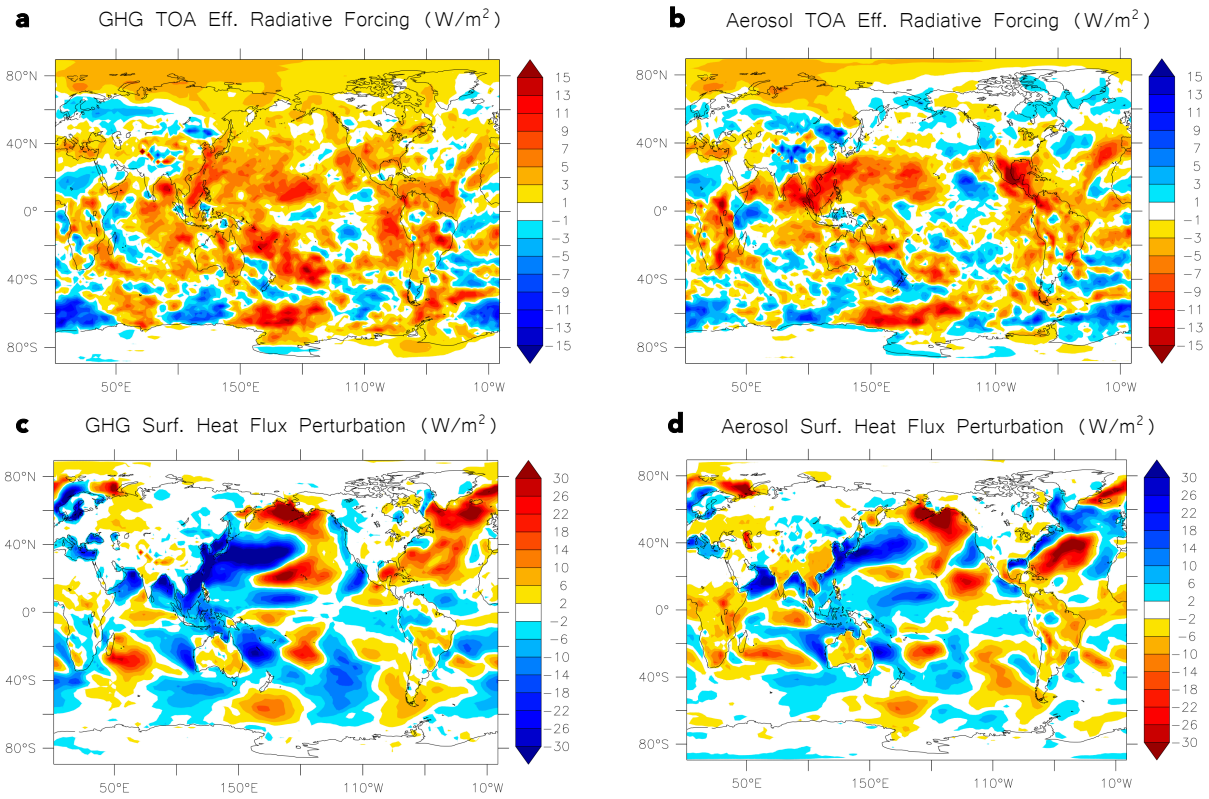

Supplementary Figure 1| Spatial Similarities in TOA and Surface Forcing. a, b, DJF-mean TOA Effective Radiative Forcing due to **(a)** GHGs and **(b)** aerosols. **c,d,** DJF-mean surface heat flux perturbation due to **(c)** GHGs and **(d)** aerosols.

	Annual Mean		**JJA**		**DJF**	
Mean of years of simulation	**1-3**	**4-7**	**1-3**	**4-7**	**1-3**	**4-7**
TOA Effective Radiative Forcing	-0.38	-0.46	-0.33	-0.41	-0.49	-0.50
Clear-sky TOA ERF	-0.15	-0.19	-0.13	-0.19	-0.48	-0.35
Tropics (20S-20N)	-0.39	-0.45	-0.44	-0.56	-0.51	-0.46
Surface Flux Perturbation	-0.43	-0.51	-0.62	-0.51	-0.37	-0.43
Tropics (20S-20N)	-0.36	-0.52	-0.54	-0.44	-0.28	-0.41
NH Extratropics (20N-90N)	-0.62	-0.58	-0.35	-0.37	-0.44	-0.40
SH Extratropics (20S-90S)	-0.29	-0.43	-0.75	-0.44	-0.32	-0.47
Surface Radiative (SW+LW) Flux	-0.28	-0.31	-0.28	-0.32	-0.41	-0.46
Surface Sensible Heat Flux	-0.56	-0.48	-0.59	-0.55	-0.44	-0.38
Surface Latent Heat Flux	-0.39	-0.44	-0.56	-0.49	-0.33	-0.44

Supplementary Table 1| Spatial correlations of TOA Effective Radiative Forcing and Surface Flux Perturbations due to greenhouse gases versus aerosols for each of the two 3-year subsets of the data.

260

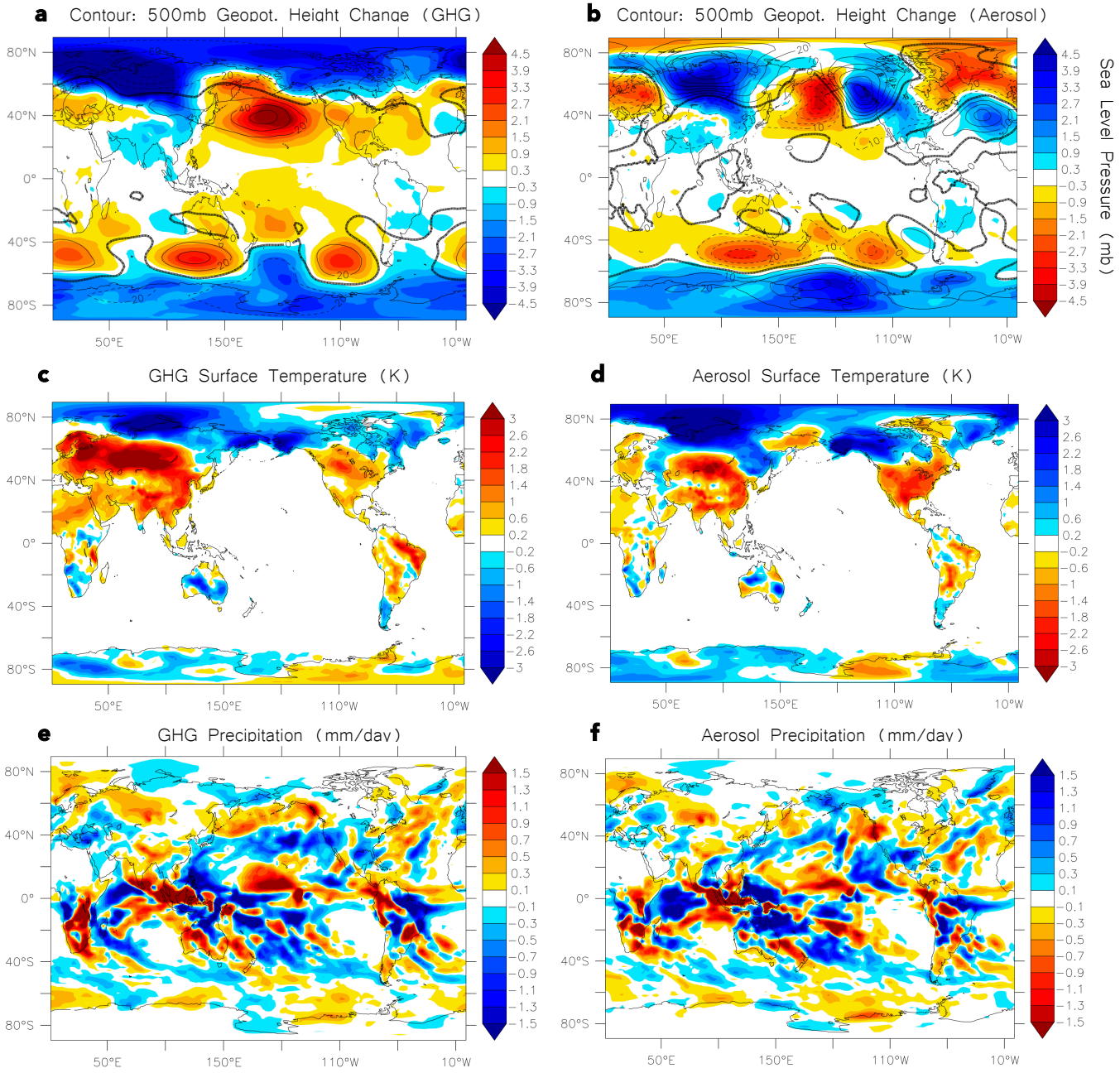

Supplementary Figure 2| Spatially similar circulation changes. a-f, DJF-mean perturbations due to **(a, c, e)** GHGs and **(b, d, f)** aerosols in **(a, b)** 500mb geopotential height (contour interval, 5 m) and sea level pressure, **(c, d)** surface temperature and **(e, f)** precipitation.